

## MoS<sub>2</sub>-CZTS: a 2D-3D nanocomposite to enhance the photocatalytic performance in degradation of methylene blue dye

R. N. Mondal<sup>a,b,\*</sup>, S. Saha<sup>b</sup>

<sup>a</sup> Dept. of Physics, Kharagpur College, Kharagpur, Paschim Medinipur, India, 721305

<sup>b</sup> Dept. of Physics, Vidyasagar University, Midnapore, Paschim Medinipur, India, 721102

Cu<sub>2</sub>ZnSnS<sub>4</sub> nanocrystals (CZTS NCs), MoS<sub>2</sub> nanosheet (NS) and MoS<sub>2</sub>-CZTS nanocomposite (NC) have been synthesized using solvothermal route. Structural characterization of samples have been done by XRD, Raman spectroscopy, HR-TEM. Samples have optically characterized by UV-Vis absorption, photoluminescence (PL) and time co-related single photon counting (TCSPC) study. The XRD, HR-TEM and Raman spectroscopy established tetragonal kesterite phase for both CZTS NCs and MoS<sub>2</sub>-CZTS NC. Enhancement of efficiency of CZTS NCs to degrade methylene blue (MB) dye, illuminated by visible light, have been observed by loading 1 wt.% MoS<sub>2</sub> NS and found to be ~100% in only 15 minutes. This is due to efficient transfer of charge carriers at p-CZTS and n-MoS<sub>2</sub> heterojunction interface, confirmed by quenching of PL intensity and decrease in average lifetime of carriers.

(Received July 2, 2024; Accepted October 4, 2024)

**Keywords:** MoS<sub>2</sub>-CZTS, Nanocomposite, Solvothermal, Heterojunction, Photocatalytic activity, Methylene blue

### 1. Introduction

The water pollution is an important issue of modern civilization. Among different industries, the textile industry is mainly responsible for water pollution because of its large consumption of water for dyeing and washing of fabrics, producing water waste containing dyes which are very harmful to living organism. MB dye is used widely in textile industry. There are different techniques to remove the organic dye from waste water like filtration, [1] chemical oxidation, [2] electrochemical treatment [3,4] etc. but adsorption [5,6] as well as photocatalysis are the most promising technique in large scale dye degradation due to its simplicity and cost-effectiveness [7–13]. Semiconducting nanomaterials have snatched attention of recent research due to their enormous catalytic applications. After absorbing light flux, a semiconductor photocatalyst generates exciton which dissociate at the defect state or interface of the semiconducting material resulting free charge carriers. This carriers decrease the electron acceptors or oxidize the donor species [14].

Copper Zinc Tin Sulfide (CZTS), a quaternary p-type semiconductor, constituting earth abundant, eco-friendly non-toxic material has attracted much more attention towards energy harvesting [15–19], thermoelectricity [20], battery application [21] as well as photocatalysis due to its optimum optical band gap value (bulk band gap is 1.5 eV) and large absorption coefficient ( $\sim 10^4$  cm<sup>-1</sup>) over solar spectrum [22–25]. Due to low band gap, there is a tendency of recombination of the free charge carriers. To overcome this problem, one of the most promising approach is to make a composite of 3D nanomaterials with 2D materials like transitional metal dichalcogenide (TMDC) because 2D materials possessing high charge carrier mobility and large surface area, dissociate the electron hole pairs easily compared to the bare 3D nanomaterials [26]. Among the TMDC, MoS<sub>2</sub> layer structured nanomaterial is the champion one because of its large charge carrier mobility ( $\sim 200$  cm<sup>2</sup> V<sup>-1</sup> S<sup>-1</sup>), dangling bond free surface and unsaturated d-orbitals of transitional metal [27,28].

---

\* Corresponding author: rudrakgpc@yahoo.com  
<https://doi.org/10.15251/CL.2024.2110.771>

However, 2D TMDC suffer from very poor light absorption ability due to its atomic level thickness, causing limited functionalities in photocatalytic application [29].

The making of composite MoS<sub>2</sub>-CZTS NC utilizes advantages of 2D materials i.e. high surface to volume ratio and large carrier mobility as well as that of the CZTS nanomaterials which comprises high optical absorption ability over solar spectrum. Gogoi et al. investigated the performance of MoS<sub>2</sub>-CZTS NC towards photocatalytic degradation of Rhodamine B organic pollutant and showed 97% degradation efficiency for 40 minutes irradiation time [30]. Shi-Jen Lin et al synthesized hydrothermally Ag/hybridized CZTS/1T-2H MoS<sub>2</sub> photocatalyst and found greater photocatalytic ability compared to the bare CZTS [31]. Enna Ha et al studied the photocatalytic activity towards hydrogen generation of CZTS/MoS<sub>2</sub>/ r-GO hybrid and showed the transportation of photoexcited electrons of CZTS to MoS<sub>2</sub> through r-GO backbone [32].

In this work, we have successfully synthesized MoS<sub>2</sub> NS using facile hydrothermal method and CZTS NC as well as MoS<sub>2</sub>-CZTS NC are grown using simple one pot solvothermal technique. The MoS<sub>2</sub>-CZTS NC shows excellent photocatalytic performance compared to bare CZTS NC and MoS<sub>2</sub> NS towards degradation of MB taken as model dye.

## 2. Experimental

### 2.1. Materials

Analytical grade Sodium molybdate dehydrate [Na<sub>2</sub>MoO<sub>4</sub>.2H<sub>2</sub>O], Copper (II) Acetate monohydrate [(CH<sub>3</sub>COO)<sub>2</sub>Cu.H<sub>2</sub>O], Zinc Nitrate hexahydrate [Zn(NO<sub>3</sub>)<sub>2</sub>.6H<sub>2</sub>O], Tin (II) Chloride dehydrate [SnCl<sub>2</sub>.2H<sub>2</sub>O] and ethylene diamine (EDA) were purchased from Merk, India. Thiourea [CH<sub>4</sub>N<sub>2</sub>S] is purchased from Himedia, India.

### 2.2. Synthesis of nanocrystals

The solvothermal process was adopted to synthesize nanomaterials as it is a single step, easy and cost effective way [33]. The morphology and dimension of the nanomaterial can be controlled by varying the solvent, surfactant and with different reaction parameters like temperature, time and pH value of the precursor solution [34].

Herein, MoS<sub>2</sub> NS is synthesized with the method used by Manikandan et al. [35]. In brief, precursor solutions were prepared by adding 0.1 M Na<sub>2</sub>MoO<sub>4</sub>.2H<sub>2</sub>O to 15 ml deionized water in one beaker and 0.6 M thiourea to another beaker containing same amount of deionized water. Both the solution were kept under stirring. After 30 minutes, thiourea solution was poured drop wise to the Na<sub>2</sub>MoO<sub>4</sub>.2H<sub>2</sub>O solution. Stirring continued for further 20 minutes. The solution was taken in a autoclave with Teflon linnig, covering with a steel jacket. Then, the sealed autoclave was transferred to a preheated furnace maintaining 200 °C for reaction time of 24 hours. Next, the autoclave was left to be cooled naturally. After cooling to RT, precipitate was centrifuged at 5000 rpm three times with double distilled water and two times with ethanol for removing by-products and unreacted ions. Finally, the precipitate was dried in air at 60 °C for 12 hours to get desired nanomaterials.

Similar strategy was taken to synthesize CZTS NCs and MoS<sub>2</sub>-CZTS NC. 30 ml solvent was prepared by water and EDA in the ratio of 3:1. 0.038 M Coppe (II) acetate monohydrate was dissolved in the 20 mL of aforesaid solution and kept under stirring. After the salt completely dissolved, 0.022 M zinc nitrate hexahydrate and 0.02 M tin (II) chloride dehydrate were added one by one to solution and stirring was continued for further 30 minutes. 10 ml 0.16 M thiourea solution was prepared separately and poured to the aforesaid solution drop wise under vigorous stirring to obtain a uniform blue coloured solution. Then, the similar step was followed as mentioned for MoS<sub>2</sub> NS synthesis. For synthesis of MoS<sub>2</sub>-CZTS NC, 1% gm-wt of MoS<sub>2</sub> NS was added to precursor solution and rest procedure was same as preparation of CZTS NCs.

### 2.3. Characterization

XRD of powder samples was performed by x-ray diffractometer (Rigaku Miniflex II using Cu K $\alpha$  radiation,  $\lambda = 0.15418$  nm) with  $2\theta$  values between 20° to 80° operated at 30 kV/10 mA. Raman spectroscopy was performed for wavenumber 200 cm<sup>-1</sup> to 700 cm<sup>-1</sup> using Raman spectrometer (LabRAM HR Evolution, Horiba) with 532 nm laser with power of 1 mW. TEM and

HR-TEM measurement was carried out by FEG-TEM (JEOL, JEM 2100F). The UV-Vis absorption study was done for wavelength ranging from 200 nm to 800 nm by Cary 5000 UV-Vis-NIR spectrophotometer and photoluminescence was characterized by fluorescence spectrophotometer (Hitachi F-7000). The photoluminescence lifetime of carriers measurement was carried out by TCSPC study (DeltaFlex, Horiba Scientific). The samples are excited with Delta Diode laser with wavelength 467 nm and decay profile is recorded with respect to time.

#### 2.4. Measurement of photocatalytic activity

Photocatalytic activity measurement of samples were executed in degrading aqueous solution of MB dye illuminated by visible light, radiated from 1000 watt halogen lamp (Phillips). 50 ml solution of MB dye in deionized water was prepared at concentration of 10 mg/L. 10 mg sample was added to that dye which was stirred at 500 rpm for 1 h under dark for adsorption desorption equilibrium. Then, the light was illuminated to dye solution containing nanomaterials with continuous constant stirring so that the photocatalyst can be uniformly illuminated. After that, 4 ml of the dye solution was taken in regular interval and centrifuged for removing nanomaterials. Degradation efficiency was investigated by measuring change of the characteristic absorbance peak height of dye solution with respect to time using UV-Vis-NIR spectrophotometer.

### 3. Results

#### 3.1. XRD analysis

XRD analysis is the basic and very important study to detect the phase and structure of a crystal. The powder XRD pattern of as grown CZTS NCs, MoS<sub>2</sub> NS and MoS<sub>2</sub>-CZTS NC are demonstrated in Fig. 1a. The x-ray peaks of CZTS NCs, positioned at 2 $\theta$  values of 28.38°, 32.87°, 47.30°, 56.10°, 69.35° and 76.41° will be indexed planes as (112), (200), (220), (312), (008) and (332) respectively. The results tally with tetragonal kesterite structure (JCPDS Card No: 26-0575) with the lattice constant values  $a = 5.43 \text{ \AA}$ ,  $b = 5.43 \text{ \AA}$  and  $c = 10.90 \text{ \AA}$  [36]. Beside this, the XRD profile of MoS<sub>2</sub> NS indicates the broadening of diffraction peaks due to weakly crystallization of as-grown nanosheets. The peaks corresponding to 2 $\theta$  values of 13.40°, 32.43°, 35.45° and 57.50° are arrived due to (002), (100), (102) and (110) planes respectively which confirms the hexagonal structure and well matched with the JCPDS Card No: 37-1592 [37]. The XRD pattern MoS<sub>2</sub>-CZTS NC reveals that there is no distinct characteristic diffraction peak corresponding to MoS<sub>2</sub> phase. This is due to the presence of very small weight ratio (1wt. %) as well as weak crystallinity of MoS<sub>2</sub> NS compared to CZTS NCs [32]. Moreover, MoS<sub>2</sub> NS does not affect the crystal phase and not produce any binary or ternary by-products. The diffraction peaks of MoS<sub>2</sub>-CZTS NC are appeared at 2 $\theta$  values of 28.69°, 33.06°, 47.58°, 56.39°, 69.50° and 76.62° corresponding to (112), (200), (220),

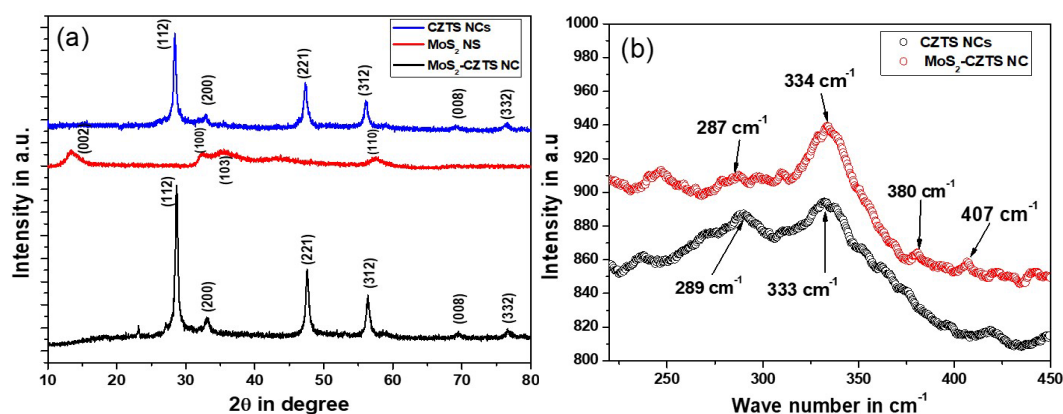


Fig. 1. (a) XRD profiles corresponding to CZTS NCs, MoS<sub>2</sub> NS and MoS<sub>2</sub>-CZTS NC; (b) Raman spectra correspond to CZTS NCs and MoS<sub>2</sub>-CZTS NC.

(312), (008) and (332) planes respectively which are very similar to the CZTS kesterite phase. The values of lattice constant are computed as  $a = b = 5.40 \text{ \AA}$  and  $c = 10.70 \text{ \AA}$ . However, the existence of  $\text{MoS}_2$  is established by Raman spectra, TEM and energy dispersive spectroscopy (EDS) elemental mapping. The average crystallite size is measured using Debye-Scherrer relation-

$$P = \frac{0.9\lambda}{\beta \cos\theta} \quad (1)$$

where  $\lambda$  is wavelength of incident Cu- $\alpha$  x-ray radiation ( $1.545 \text{ \AA}$ ).  $\beta$  is full width at half maxima (FWHM) and  $\theta$  is Bragg angle. The approximate crystal size is computed as  $\sim 19.98 \text{ nm}$  and  $\sim 20.49 \text{ nm}$  for CZTS NCs and  $\text{MoS}_2$ -CZTS NC respectively, which consequences that the presence of small amount of  $\text{MoS}_2$  NS does not influence the particle size effectively.

### 3.2. Raman spectroscopy

Raman measurement is important for structural homogeneity of as-synthesized crystal. Furthermore, in case of chalcogenides based quaternary semiconducting nanomaterials, it is necessary to perform Raman measurement because there is a probability of growing binary and ternary secondary phases and XRD profile of those phases are too close to desired kesterite phase to identify distinctly. Fig. 1b depicts the Raman spectra of CZTS NCs and  $\text{MoS}_2$ -CZTS NC. The characteristic peak at  $333 \text{ cm}^{-1}$  along with a secondary peak at  $289 \text{ cm}^{-1}$  are arrived for CZTS NC, which confirm the kesterite phase. The peak at  $333 \text{ cm}^{-1}$  is due to A mode of sulphur around the metal atoms and the peak at  $289 \text{ cm}^{-1}$  is because of the longitudinal optical (LO) mode vibration of cations [38]. Apparently, for  $\text{MoS}_2$ -CZTS NC, beside two CZTS peaks at  $287$  and  $334 \text{ cm}^{-1}$ , two additional peaks with small intensity are found at  $380$  and  $407 \text{ cm}^{-1}$ , which are characteristic peaks, originating due to the  $E_{2g}^1$  and  $A_{1g}$  mode of 2H phase semiconducting  $\text{MoS}_2$  respectively [39]. The peak at  $\sim 380 \text{ cm}^{-1}$  ( $E_{2g}^1$  mode) is for in-plane mode vibration of molybdenum and sulphur atoms in opposite direction to each other. The peak at  $\sim 407 \text{ cm}^{-1}$  is for out-of-plane vibration of those atoms. No peaks are found corresponding to any unwanted binary and/or ternary phase in Raman spectra of CZTS NCs and also in  $\text{MoS}_2$ -CZTS NC, indicating the purity of as-synthesized samples. Raman data also reveals that the coexistence of  $\text{MoS}_2$  and CZTS into the as-synthesized  $\text{MoS}_2$ -CZTS NC, which could not be attributed by the XRD measurement.

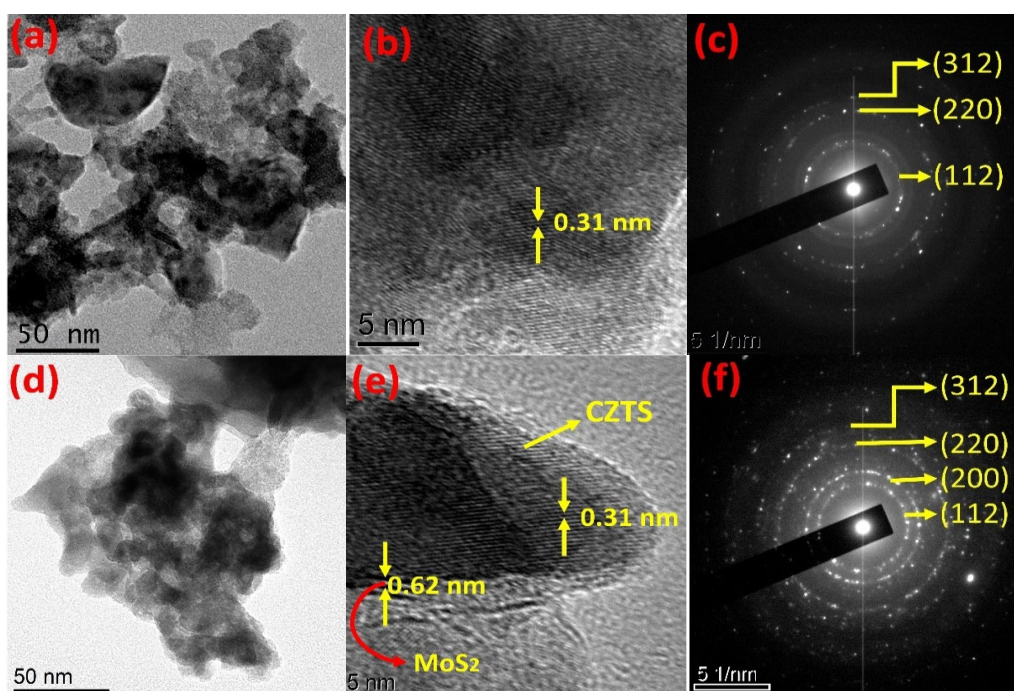


Fig. 2 (a-c) TEM, HRTEM and SAED images corresponding to CZTS NCs; (d-f) TEM, HRTEM and SAED images correspond to  $\text{MoS}_2$ -CZTS NC.

### 3.3. TEM and HRTEM analysis

TEM measurement is important to determine morphology, crystal structure and crystallite size of nanomaterial. Fig. 2 illustrates the TEM, HR-TEM and SAED pattern of as grown CZTS NCs and MoS<sub>2</sub>-CZTS NC. The particle distribution of CZTS NCs and MoS<sub>2</sub>-CZTS NC are shown in Fig. 2a and Fig. 2d respectively and the crystallite size is ~17 nm and ~19 nm. The values of interplanar spacing are found to be 0.31 nm of both samples for (112) plane obtained from Fig. 2b and Fig. 2e. The SAED pattern of CZTS NCs and MoS<sub>2</sub>-CZTS NC are displayed in Fig. 2c and Fig. 2f respectively. The distinct circular rings indicate the diffraction from different planes. In case of CZTS NCs, the ring corresponding to (200) diffraction plane is absent, which may be attributed to the very weak intensity corresponding to this plane as seen in XRD profile. Fig. 2e clearly indicates that the formation of MoS<sub>2</sub>-CZTS NC where nanocrystalline CZTS are grown over 2D MoS<sub>2</sub> NS. Hence, in-situ heterojunctions are formed by n-type MoS<sub>2</sub> and p-type CZTS. Additionally, the heterojunctions offer large interfacial contact area which is highly recommended for superior charge carrier transfer as well as for obstructing carrier recombination. These are the significant conditions to enhance the photocatalytic activity. The EDS elemental mapping is performed to confirm the existence of different elements in the MoS<sub>2</sub>-CZTS NC. Fig. 3a shows the area selected for elemental mapping and Fig. (3b – 3f) depict the HAADF images of MoS<sub>2</sub>-CZTS NC which show mapping of Cu, Zn, Sn, S and Mo atoms respectively illustrating well distribution of all the elements.

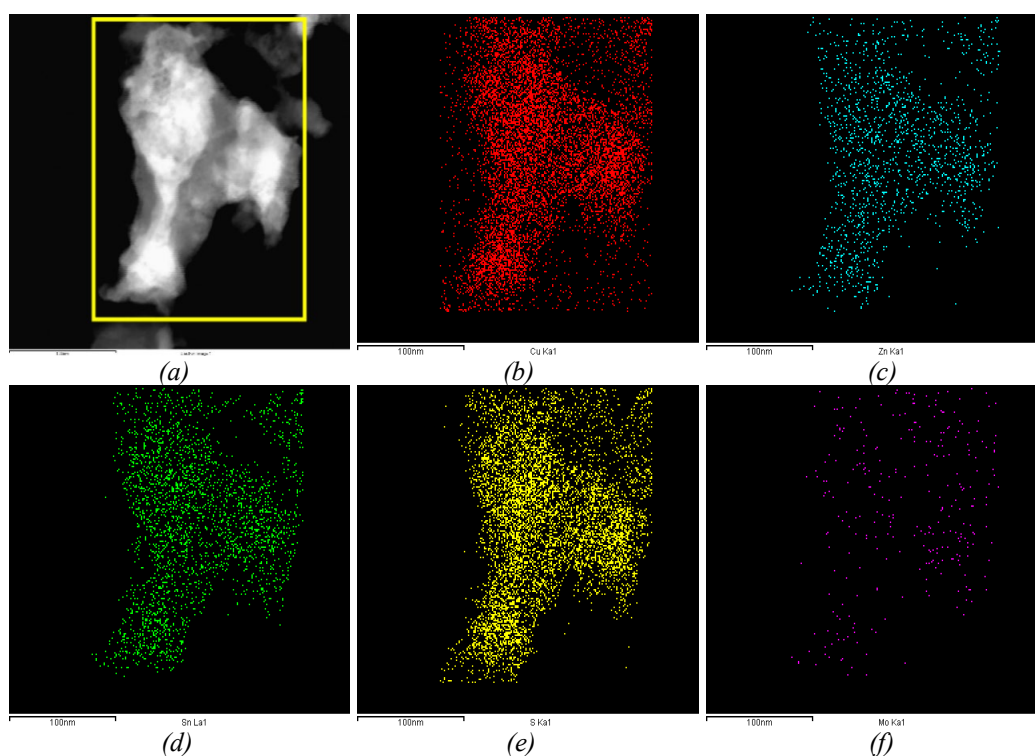


Fig. 3. HAADF images corresponding to MoS<sub>2</sub>-CZTS NCs shows well distribution of individual elements; (a – selected area of MoS<sub>2</sub>-CZTS NC; b – copper; c – zinc; d – tin; e – sulfur and f – Molybdenum).

### 3.4. Optical absorption property

The optical absorption study is essential to determine the band gap values and also to investigate the ability of the nanomaterials in the field of photocatalysis and photovoltaic applications under solar spectrum. The absorption spectrum are recorded in 200 to 800 nm wavelength range and Fig. (4a - 4c) demonstrate the variation of absorbance of MoS<sub>2</sub> NS, CZTS NCs and MoS<sub>2</sub>-CZTS NC respectively. It is clearly seen that the absorbance is affected significantly while loading of MoS<sub>2</sub> NS for synthesizing MoS<sub>2</sub>-CZTS NC. The band gap values are calculated using Tauc equation for direct band gap materials-

$$(\alpha h\nu)^2 = C(h\nu - E_g) \quad (2)$$

where  $\alpha$  is the optical absorption co-efficient,  $C$  is constant and  $E_g$  is optical band gap. The inset to Fig. (4a and 4b) display the variation of  $(\alpha h\nu)^2$  with respect to photon energy ( $h\nu$ ). By extrapolating the linear segment of the graph on the x axis (photon energy), the band gaps are estimated. The band gaps are found to be 1.51 eV for MoS<sub>2</sub> NS and 1.67 eV for CZTS NC. The enhancement in band gap for CZTS NC compared to bulk counterpart is attributed to size reduction of the materials [40]. For MoS<sub>2</sub>, band gap value depends on the layer number [41]. The band gap is 1.8 eV for monolayer MoS<sub>2</sub>, whereas, it is 1.2 eV for bulk counterpart. The estimated values of band gap are well matched with the literature [30,42–44].

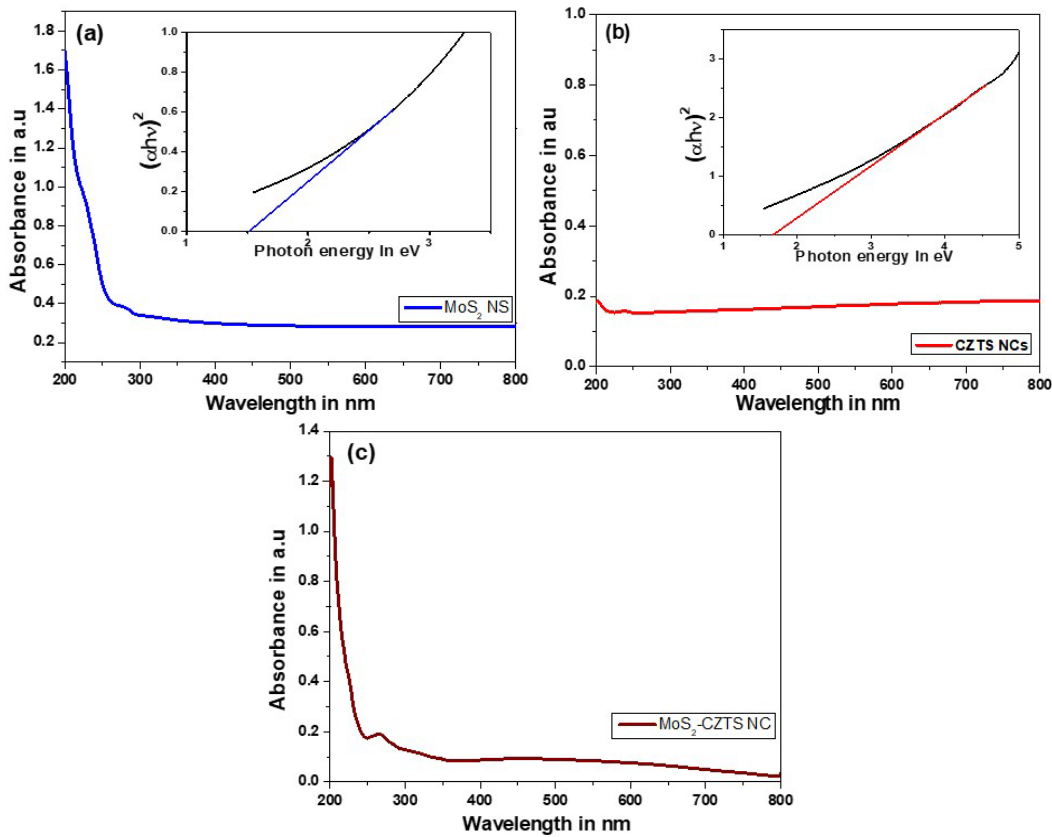


Fig. 4. Absorbance spectra of (a) MoS<sub>2</sub> NS, (b) CZTS NCs (inset showing Tauc plot to determine band gap) and (c) MoS<sub>2</sub>-CZTS NC.

### 3.5. Photoluminescence and TCSPC study

The study of photoluminescence (PL) properties is an effective and important method to detect impurity or defect states present in the synthesized samples. It also give information about charge transfer mechanism in heterostructure. PL spectra of CZTS NCs and MoS<sub>2</sub>-CZTS NC using 710 nm excitation are illustrated in Fig. 5a. Apparently, there are two peaks arrived for bare CZTS NC. The peak, arrived at 751 nm is due to transition of electrons between bands. Besides, the high intensified peak, positioned at 791 nm is due to the electron transition from the defect states present near the conduction band to the valence band. On the other hand, only one small peak around 749 nm is observed while loading MoS<sub>2</sub> NS to CZTS. The PL intensity is fully quenched around 791 nm implying the transportation of photoexcited electrons from the conduction band of CZTS NCs to the conduction band of MoS<sub>2</sub> NS which is favorable for photocatalytic application [45].

The charge transfer phenomenon is also established by time co-related single photon counting (TCSPC) spectra. The photoluminescence lifetime of the carriers is calculated by decay data fitting with multi exponential equation- [46]

$$I(t) = I_0 \sum_{n=1}^N A_n e^{-t/T_n} \quad (3)$$

$$T_{av} = \frac{\sum A_n T_n}{\sum A_n} \quad (4)$$

where,  $I_0$  is the number of initial photons,  $A_n$  is the pre-exponential factor indicating the percentage of the initial number of photons with lifetime  $T_n$ . The photoluminescence decay curve of CZTS NC and MoS<sub>2</sub>-CZTS NC with excitation 467 nm and emission 700 nm is demonstrated in Fig. 5b and Fig. 5c respectively. The decay curve of CZTS NCs is fitted well with bi-exponential function, whereas, the decay data of MoS<sub>2</sub>-CZTS NC is fitted with tri-exponential function. The fitting parameters have been displayed in Table 1. Additionally, The residuals vs. time plot with  $\chi^2$  values (1.17 for CZTS NCs and 1.19 for MoS<sub>2</sub>-CZTS NC) are illustrated in Fig. 5d and 5e. The values of the average lifetime are estimated using equation (4) and found to be 0.19 ns and 0.13 ns for CZTS NCs and MoS<sub>2</sub>-CZTS NC respectively. The reducing in average lifetime of the carriers reveals that the photo-induced charge transfer occurred at the CZTS NCs to MoS<sub>2</sub> NS interface which confirms the quenching phenomenon of the PL spectra [47,48].

Table 1. Parameters to calculate average photoluminescence lifetime of carriers.

Sample	A <sub>1</sub> (%)	A <sub>2</sub> (%)	A <sub>3</sub> (%)	T <sub>1</sub> (ns)	T <sub>2</sub> (ns)	T <sub>3</sub> (ns)	Average Lifetime (ns)
CZTS NC	97	3	-	0.12032	2.71528	-	0.19
MoS <sub>2</sub> -CZTS NC	48.4	48.4	3.2	0.10142	0.10142	1.27506	0.13

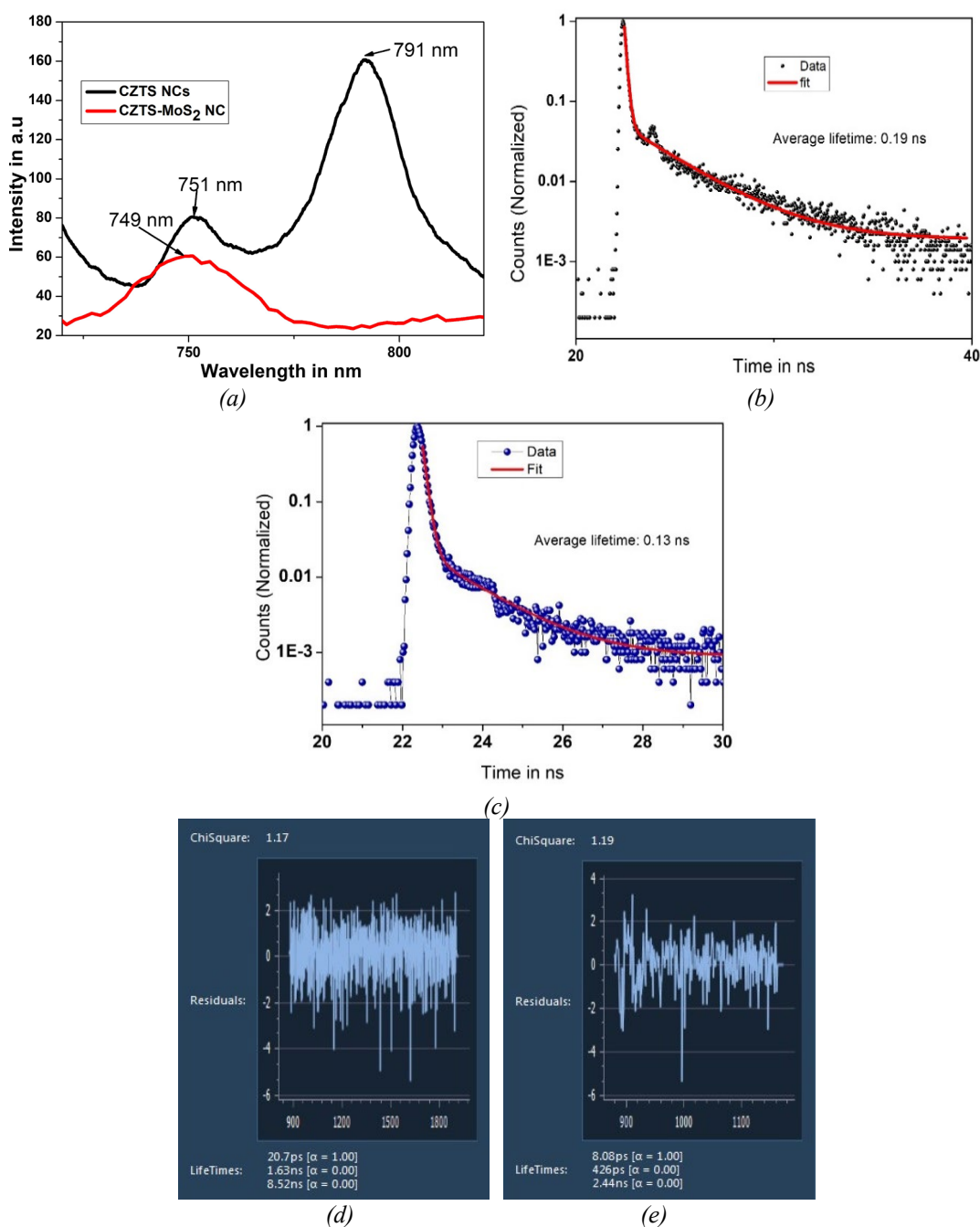


Fig. 5. (a) PL spectra, TCSPC decay spectra of (b) CZTS NCs and (c) MoS<sub>2</sub>-CZTS NC; Residuals vs. time (ns) plot with  $\chi^2$  of (d) - CZTS NCs and (e) - MoS<sub>2</sub>-CZTS NC.

### 3.6. Photocatalytic activity

The photocatalytic potential of as-synthesized nanomaterials are displayed in the Fig. 6 where we have studied the absorbance of the aqueous solution of MB dye as a function of wavelength which reflects the degradation mechanism under illumination of visible light. MB is one of the azo dye which reveals major absorbance bands at 293 nm ( $\pi$ - $\pi^*$  transition) and 663 nm ( $n$ - $\pi^*$  transition) for UV-Visible absorption spectra. There is another peak, like shoulder of peak positioned at 663 nm, appeared at 610 nm must be due to 0-1 vibronic transition [49]. Here, we have focused only the main characteristic peak positioned at 663 nm. This absorbance profile of MB is almost unchanged over a period of 12 hours under illumination of light suggesting that the MB dye itself is stable and cannot be degraded over time. It is observed that the peak height gradually decreases with

time under illumination in presence of MoS<sub>2</sub> NS, CZTS NCs and MoS<sub>2</sub>-CZTS NC shown in Fig. (6a-6c) respectively. It seems that the dye is degraded with time effectively in presence of nanomaterials, act as photocatalyst, under illumination of visible light. The percentage of degradation or degradation efficiency is computed using following equation [50]-

$$\% \text{ of degradation} = \frac{C_0 - C}{C_0} \times 100 \quad (5)$$

where  $C_0$  and  $C$  represent the initial concentration of MB dye and the concentration at any instant  $t$  respectively. The degradation efficiencies are estimated as  $\sim 70\%$  and  $\sim 92\%$  for MoS<sub>2</sub> NS and CZTS NCs respectively under illumination of light for 60 minutes whereas, for MoS<sub>2</sub>-CZTS NC it is found to be  $\sim 100\%$  for 15 minutes irradiation time only. The photocatalytic degradation kinetics was also studied to investigate degradation mechanism. The degradation of MB dye obeys pseudo first order reaction. The rate constant ( $k$ ) is attributed from the relation [51]-

$$\ln\left(\frac{C}{C_0}\right) = -kt \quad (6)$$

Fig. 6d illustrates time vs.  $\ln(C/C_0)$  graph alongwith linear fitting of the data. The linear nature of graph confirms the first order reaction kinetics of the photocatalytic degradation process. The  $k$  values are found to be 0.02924, 0.04844 and 0.28285  $\text{min}^{-1}$  for MoS<sub>2</sub> NS, CZTS NCs and MoS<sub>2</sub>-CZTS NC respectively.

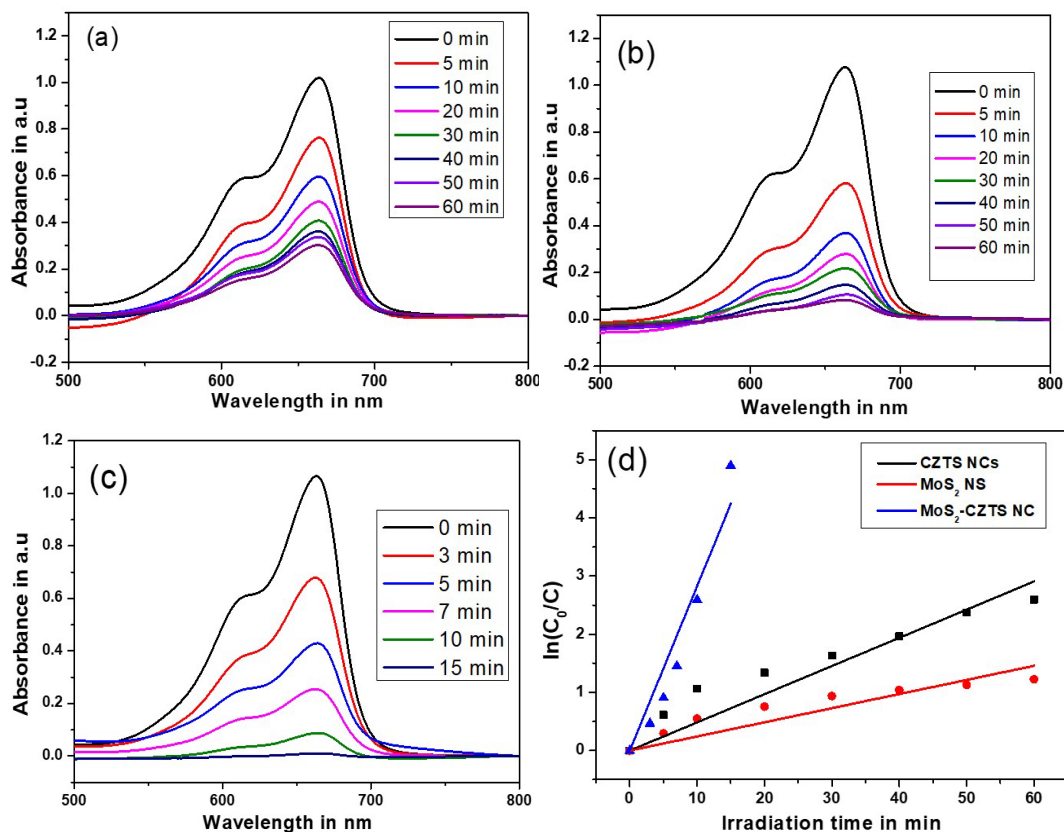


Fig. 6. Absorbance spectra of aqueous solution of MB dye in presence of (a) MoS<sub>2</sub> NS, (b) CZTS NCs and (c) MoS<sub>2</sub>-CZTS NC under illumination of visible light; (d)  $\ln\frac{C_0}{C}$  vs time graph to determine rate constant.

Apparently, MoS<sub>2</sub> NS and CZTS NCs exhibit good photocatalytic behaviour but CZTS loaded with MoS<sub>2</sub> NS shows excellent performance towards visible light driven degradation of organic dyes. When visible light is irradiated to semiconducting material with suitable band gap, the

excitons are generated and separated into free electrons ( $e^-$ ) and holes ( $h^+$ ). In bare CZTS NCs and MoS<sub>2</sub> NS, there is a tendency of recombination of those photogenerated  $e^-$  and  $h^+$  which inhibits the photocatalytic performance. On the other hand, excellent photocatalytic performance is observed for MoS<sub>2</sub>-CZTS NC. This can be attributed to more active sites present in MoS<sub>2</sub>-CZTS NC to make reaction with aqueous solution of dye and there is a pathway of charge transfer in the junction of CZTS and MoS<sub>2</sub> which is due to preferable band alignment as shown in schematic diagram (Fig. 7).

The charge transfer mechanism of the heterojunction under illumination of light is illustrated as follows. Fig. 7 represents the equilibrium condition of n-MoS<sub>2</sub>/p-CZTS heterojunction where the Fermi energy ( $E_F$ ) is same for both sides. The depletion region (shaded with blue colour) is formed in the heterojunction in which a built-in electric field is created. The values of electron affinity ( $\chi$ ) of the n-MoS<sub>2</sub> NS and p-CZTS NCs are 4.3 eV and 3.7 eV respectively which make suitable band alignment for transferring charge carriers [52,53]. Under irradiation of visible light, which is obviously having greater energy than the band gap energy values of both CZTS NCs and MoS<sub>2</sub> NS, electrons of VB of both sides (p and n) can undergo a transition to CB leaving holes. Hence, photogenerated charge carriers are formed which move in opposite directions i.e. electrons travel towards n-MoS<sub>2</sub> side and holes to p-CZTS because of built-in field and suitable bending of band [54]. Thus it resists the  $e^-$  and  $h^+$  recombination. The occurrence of charge separation is confirmed by quenching phenomenon of PL intensity (Fig. 5a) and also decrease in PL lifetime (Fig. 5b and Fig. 5c), while making composite CZTS NCs with MoS<sub>2</sub> NS. Furthermore, the high absorption coefficient of CZTS NCs enhances the photogenerated charge carrier concentration. Moreover, the high charge carrier mobility of MoS<sub>2</sub> NS as well as high quality junction of CZTS and MoS<sub>2</sub> (Fig. 2e) accelerate the charge separation process which consequences greater number of  $e^-$  and  $h^+$  in the MoS<sub>2</sub>-CZTS NC. Additionally, MoS<sub>2</sub> NS offers two dimensional sheet for CZTS NC to prevent themselves from agglomeration which results stable and well uniform dispersion of nanomaterials in the solvent.

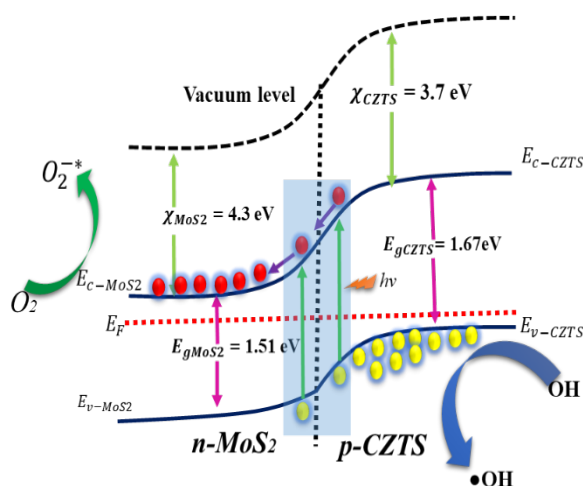
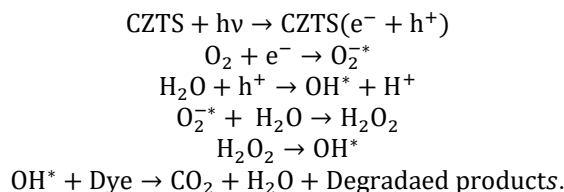


Fig. 7. Schematic of band alignment MoS<sub>2</sub>-CZTS NC and photocatalytic mechanism.

The dye degradation mechanism can be explained as follows. Under illumination of light, the photogenerated holes and electrons move to the surface of the semiconducting photocatalysts (MoS<sub>2</sub> NS, CZTS NCs and MoS<sub>2</sub>-CZTS NC) where they can undergo redox reaction with the organic pollutant. The electrons may reduce the adsorbed oxygen which is available in the surface of the photocatalyst, to the superoxide radical anion  $O_2^{\cdot-}$ . The holes can easily make reaction with water at the photocatalyst surface and generate hydroxyl radical  $OH^{\cdot}$ , which is responsible mostly for dye degradation. The superoxide  $O_2^{\cdot-}$  can further undergo a reaction with  $H_2O$  and producing  $H_2O_2$  which may degraded to  $OH^{\cdot}$ . Finally,  $OH^{\cdot}$  radical degrades dye by producing  $CO_2$  and  $H_2O$  with byproducts. The possible reactions are as follows-



#### 4. Conclusion

In summary, TEM, Photoluminescence as well as Raman spectra clearly indicate the formation of MoS<sub>2</sub>-CZTS nanocomposite. Individually CZTS NC is better than MoS<sub>2</sub> NS as far as photocatalytic activity in degradation of MB dye is concerned. CZTS NC is also not found to be very efficient in this respect. But MoS<sub>2</sub>-CZTS NC presents itself as one of the promising 2D-3D composite material in the field of the photocatalytic dye degradation. In this paper we have established the capability of MoS<sub>2</sub>-CZTS nanocomposite (NC) as an efficient catalyst in the visible light for photocatalysis applications.

#### Acknowledgements

The authors are greatly thankful to the Department of Physics, Vidyasagar University. The authors are also acknowledging USIC, Vidyasagar University for certain instrumental facilities. Authors further acknowledge CRF, IIT KGP and CSS, IACS Kolkata for various characterization facilities.

#### References

- [1] K. Sunil, P. Sherugar, S. Rao, C. Lavanya, G.R. Balakrishna, G. Arthanareeswaran, M. Padaki, *J. Environ. Chem. Eng.* 9 (2021) 106328; <https://doi.org/10.1016/j.jece.2021.106328>
- [2] K. Dutta, S. Mukhopadhyay, S. Bhattacharjee, B. Chaudhuri, *J. Hazard. Mater.* 84 (2001) 57-71; [https://doi.org/10.1016/S0304-3894\(01\)00202-3](https://doi.org/10.1016/S0304-3894(01)00202-3)
- [3] A.Y. Goren, Y.K. Recepoğlu, Ö. Edebali, C. Sahin, M. Genisoglu, H.E. Okten, *ACS Omega* 7 (2022) 32640-32652; <https://doi.org/10.1021/acsomega.2c04304>
- [4] M.R. Samarghandi, A. Dargahi, A. Shabanloo, H.Z. Nasab, Y. Vaziri, A. Ansari, *Arab. J. Chem.* 13 (2020) 6847-6864; <https://doi.org/10.1016/j.arabjc.2020.06.038>
- [5] Y. Miyah, A. Lahrichi, M. Idrissi, A. Khalil, F. Zerrouq, *Surfaces and Interfaces* 11 (2018) 74-81; <https://doi.org/10.1016/j.surfin.2018.03.006>
- [6] J. Cheng, C. Zhan, J. Wu, Z. Cui, J. Si, Q. Wang, X. Peng, L.S. Turng, *ACS Omega* 5 (2020) 5389-5400; <https://doi.org/10.1021/acsomega.9b04425>
- [7] C.W. Lai, J.C. Juan, W.B. Ko, S. Bee Abd Hamid, *Int. J. Photoenergy* 2014 (2014); <https://doi.org/10.1155/2014/524135>
- [8] A.P. Chowdhury, K.S. Anantharaju, K. Keshavamurthy, S.L. Rokhum, *J. Chem.* 2023 (2023); <https://doi.org/10.1155/2023/9780955>
- [9] T. Shindhal, P. Rakholiya, S. Varjani, A. Pandey, H.H. Ngo, W. Guo, H.Y. Ng, M.J. Taherzadeh, *Bioengineered* 12 (2021) 70-87; <https://doi.org/10.1080/21655979.2020.1863034>
- [10] G. Anandhi, M. Iyapparaja, *RSC Adv.* 14 (2024) 9003-9019; <https://doi.org/10.1039/D4RA00711E>
- [11] M. Boonkam, P. Tamdee, P. Tongying, *Chalcogenide Lett.* 21 (2024) 335-342; <https://doi.org/10.15251/CL.2024.214.335>
- [12] M.A. Hassaan, M.A. El-Nemr, M.R. Elkatory, S. Ragab, V.C. Niculescu, A. El Nemr, *Top. Curr. Chem.* 381 (2023) 31; <https://doi.org/10.1007/s41061-023-00444-7>
- [13] S. Khan, T. Noor, N. Iqbal, L. Yaqoob, *ACS Omega* (2024) 21751-21767.

- [14] Z. Kalaycıoğlu, B. Özüğür Uysal, Ö. Pekcan, F.B. Erim, ACS Omega 8 (2023) 13004-13015; <https://doi.org/10.1021/acsomega.3c00198>
- [15] W. Wang, M.T. Winkler, O. Gunawan, T. Gokmen, T.K. Todorov, Y. Zhu, D.B. Mitzi, Adv. Energy Mater. 4 (2013) 1-5; <https://doi.org/10.1002/aenm.201301465>
- [16] X. Zhang, E. Fu, Y. Wang, C. Zhang, Nanomaterials 9 (2019) 336; <https://doi.org/10.3390/nano9030336>
- [17] S. Tajima, T. Itoh, H. Hazama, K. Ohishi, R. Asahi, Appl. Phys. Express 8 (2015) 082302; <https://doi.org/10.7567/APEX.8.082302>
- [18] A. Almohammed, E.R. Shaaban, Chalcogenide Lett. 19 (2022) 701-714; <https://doi.org/10.15251/CL.2022.1910.701>
- [19] V.M.H. Cao, J. Bae, J. Shim, B. Hong, H. Jee, J. Lee, Appl. Sci. 12 (2022) 38; <https://doi.org/10.3390/app12010038>
- [20] U. Syafiq, E. Isotta, N. Ataollahi, K. Lohani, S. Luong, V. Trifiletti, O. Fenwick, P. Scardi, ACS Appl. Energy Mater. 5 (2022) 5909-5918; <https://doi.org/10.1021/acsaem.2c00268>
- [21] Z. Syum, T. Billo, A. Sabbah, B. Venugopal, S.Y. Yu, F.Y. Fu, H.L. Wu, L.C. Chen, K.H. Chen, ACS Sustain. Chem. Eng. 9 (2021) 8970-8979; <https://doi.org/10.1021/acssuschemeng.1c01341>
- [22] N. Kamoun, H. Bouzouita, B. Rezig, Thin Solid Films 515 (2007) 5949-5952; <https://doi.org/10.1016/j.tsf.2006.12.144>
- [23] R. Touati, M. Ben Rabeh, M. Kanzari, Energy Procedia 44 (2014) 44-51; <https://doi.org/10.1016/j.egypro.2013.12.008>
- [24] M.I. Hossain, Chalcogenide Lett. 9 (2012) 231-242.
- [25] A. Paraye, R. Manivannan, S.N. Victoria Selvam, Chalcogenide Lett. 17 (2020) 77-83; <https://doi.org/10.15251/CL.2020.172.77>
- [26] S. Maity, K. Sarkar, P. Kumar, ACS Appl. Nano Mater. 6 (2023) 4224-4235; <https://doi.org/10.1021/acsnm.2c05314>
- [27] H.S. Nalwa, RSC Adv. 10 (2020) 30529-30602; <https://doi.org/10.1039/D0RA03183F>
- [28] S. Kim, A. Konar, W.S. Hwang, J.H. Lee, J. Lee, J. Yang, C. Jung, H. Kim, J.B. Yoo, J.Y. Choi, Y.W. Jin, S.Y. Lee, D. Jena, W. Choi, K. Kim, Nat. Commun. 3 (2012) 1011; <https://doi.org/10.1038/ncomms2018>
- [29] H. Li, M. Qin, L. Wang, X. Zhai, R. Ren, J. Hu, Opt. Express 25 (2017) 31612; <https://doi.org/10.1364/OE.25.031612>
- [30] G. Gogoi, S. Arora, N. Vinothkumar, M. De, M. Qureshi, RSC Adv. 5 (2015) 40475-40483; <https://doi.org/10.1039/C5RA03401A>
- [31] S.J. Lin, J.M. Ting, K.C. Hsu, Y.S. Fu, Materials (Basel). 11 (2018) 1-13; <https://doi.org/10.3390/ma11010158>
- [32] E. Ha, W. Liu, L. Wang, H.W. Man, L. Hu, S.C.E. Tsang, C.T.L. Chan, W.M. Kwok, L.Y.S. Lee, K.Y. Wong, Sci. Rep. 7 (2017) 1-8; <https://doi.org/10.1038/s41598-016-0028-x>
- [33] S. Das, I. Alam, J. Raiguru, B.V.R.S. Subramanyam, P. Mahanandia, Phys. E Low-Dimensional Syst. Nanostructures 105 (2019) 19-24; <https://doi.org/10.1016/j.physe.2018.08.020>
- [34] A.G. Kannan, T.E. Manjulavalli, J. Chandrasekaran, in: Procedia Eng., Elsevier Ltd, 2016, pp. 15-22; <https://doi.org/10.1016/j.proeng.2015.08.1112>
- [35] R. Manikandan, G. Raina, Phys. Scr. 97 (2022); <https://doi.org/10.1088/1402-4896/ac9d6f>
- [36] W.C. Liu, B.L. Guo, X.S. Wu, F.M. Zhang, C.L. Mak, K.H. Wong, J. Mater. Chem. A 1 (2013) 3182-3186; <https://doi.org/10.1039/c3ta00357d>
- [37] P. Basu, J. Chakraborty, N. Ganguli, K. Mukherjee, K. Acharya, B. Satpati, S. Khamrui, S. Mandal, D. Banerjee, D. Goswami, P.M.G. Nambissan, K. Chatterjee, ACS Appl. Mater. Interfaces 11 (2019) 48179-48191; <https://doi.org/10.1021/acsmi.9b12988>

- [38] Y. Havryliuk, M.Y. Valakh, V. Dzhagan, O. Greshchuk, V. Yukhymchuk, A. Raevskaya, O. Stroyuk, O. Selyshchev, N. Gaponik, D.R.T. Zahn, RSC Adv. 8 (2018) 30736-30746; <https://doi.org/10.1039/C8RA05390A>
- [39] T. Livne, Y. Yechezkel, A.K. Sarkar, I. Zucker, ACS Sustain. Chem. Eng. 10 (2022) 10417-10425; <https://doi.org/10.1021/acssuschemeng.2c03596>
- [40] F.T. Rabouw, C. de Mello Donega, Top. Curr. Chem. 374 (2016) 1-30; <https://doi.org/10.1007/s41061-015-0002-2>
- [41] X. Li, H. Zhu, J. Mater. 1 (2015) 33-44; <https://doi.org/10.1016/j.jmat.2015.03.003>
- [42] A. Tumbul, A. Göktaş, M.Z. Zarbali, F. Aslan, Mater. Res. Express 5 (2018) 066408; <https://doi.org/10.1088/2053-1591/aac80e>
- [43] C.P. Veeramalai, F. Li, Y. Liu, Z. Xu, T. Guo, T.W. Kim, Appl. Surf. Sci. 389 (2016) 1017-1022; <https://doi.org/10.1016/j.apsusc.2016.08.031>
- [44] A. Chaves, J.G. Azadani, H. Alsalman, D.R. da Costa, R. Frisenda, A.J. Chaves, S.H. Song, Y.D. Kim, D. He, J. Zhou, A. Castellanos-Gomez, F.M. Peeters, Z. Liu, C.L. Hinkle, S.H. Oh, P.D. Ye, S.J. Koester, Y.H. Lee, P. Avouris, X. Wang, T. Low, Npj 2D Mater. Appl. 4 (2020) 29; <https://doi.org/10.1038/s41699-020-00162-4>
- [45] K. Chakraborty, T. Pal, S. Ghosh, ACS Appl. Nano Mater. 1 (2018) 3137-3144; <https://doi.org/10.1021/acsanm.8b00295>
- [46] J.R. Lakowicz, Principles of Fluorescence Spectroscopy, Third, Springer Book, Baltimore, USA, 2006; <https://doi.org/10.1007/978-0-387-46312-4>
- [47] S. Maity, K. Sarkar, P. Kumar, Nanoscale 15 (2023) 16068-16079; <https://doi.org/10.1039/D3NR03754A>
- [48] X. Wen, P. Yu, Y.R. Toh, Y.C. Lee, K.Y. Huang, S. Huang, S. Shrestha, G. Conibeer, J. Tang, J. Mater. Chem. C 2 (2014) 3826-3834; <https://doi.org/10.1039/C3TC32376E>
- [49] D. Heger, J. Jirkovský, P. Klán, J. Phys. Chem. A 109 (2005) 6702-6709; <https://doi.org/10.1021/jp050439j>
- [50] P. Kush, K. Deori, A. Kumar, S. Deka, J. Mater. Chem. A 3 (2015) 8098-8106; <https://doi.org/10.1039/C4TA06551D>
- [51] J. Fowsiya, G. Madhumitha, N.A. Al-Dhabi, M.V. Arasu, J. Photochem. Photobiol. B Biol. 162 (2016) 395-401; <https://doi.org/10.1016/j.jphotobiol.2016.07.011>
- [52] A. Nourbakhsh, A. Zubair, R.N. Sajjad, T.K.G. Amir, W. Chen, S. Fang, X. Ling, J. Kong, M.S. Dresselhaus, E. Kaxiras, K.K. Berggren, D. Antoniadis, T. Palacios, Nano Lett. 16 (2016) 7798-7806; <https://doi.org/10.1021/acs.nanolett.6b03999>
- [53] S. Singh, A.K. Katiyar, A. Midya, A. Ghorai, S.K. Ray, Nanotechnology 28 (2017) 435704; <https://doi.org/10.1088/1361-6528/aa81dd>
- [54] J.S. Jang, H.G. Kim, J.S. Lee, Catal. Today 185 (2012) 270-277; <https://doi.org/10.1016/j.cattod.2011.07.008>